

# BEAM BEHAVIOR THROUGH THE SNS CHOPPER SYSTEM\*

S. Nath, J. Billen, J. Stovall, H. Takeda, L. Young, LANL, Los Alamos, NM 87545, USA,  
D. Jeon, S. H. Kim, SNS/ORNL, Oak Ridge, USA, and K. Crandall, Tech Source, Santa Fe, NM  
87501, USA

## Abstract

The Spallation Neutron Source (SNS) linac consists of a 2.5-MeV RFQ, a Medium Energy Beam Transfer (MEBT) line, a 402.5-MHz DTL, followed by 805-MHz CCL and SRF structures that accelerate beam to a final energy of 1 GeV. It is designed to inject 1.4 mA average  $H^-$  beam into the storage ring. To minimize beam loss during ring extraction we “chop” a 300-ns notch out of the beam at 1 MHz. This notch is preserved throughout the linac and ring filling to provide a clean extraction gap.

Chopping is accomplished in two stages. A segmented Einzel-lens in the low-energy beam transport (LEBT) line chops the beam by deflecting it between the RFQ vanes. A traveling-wave parallel-plate structure in the MEBT deflects beam vertically onto a target. By design, [1] this chopping system provides a gap to beam current ratio of  $10^{-4}$ . In this paper, we investigate four chopper-timing scenarios and examine the expected beam behavior.

## 1 INTRODUCTION

The SNS linac [2] injects a 1.4-MW  $H^-$  beam into an accumulator ring with the pulse structure shown in Fig. 1. The beam duty factor is 6%: 1-ms macropulses at 60 Hz. The chopping breaks each macropulse into 1060 minipulses separated by 300-ns gaps, thus passing 68% of the beam. These minipulses stack up in the ring, creating a single extraction gap. A minipulse contains 260 micropulses bunched in the RFQ at 402.5 MHz. In two stages, we remove (chop)  $\sim 120$  micropulses to create the 300-ns gap. A segmented Einzel-lens (LEBT chopper) just before the RFQ deflects beam between the RFQ vanes, and a traveling-wave MEBT chopper deflects beam vertically onto a target. Because of the several-ns rise and fall times of the chopper voltage, the edges of the beam gap are “contaminated” with partially chopped micropulses whose destiny is somewhat uncertain.

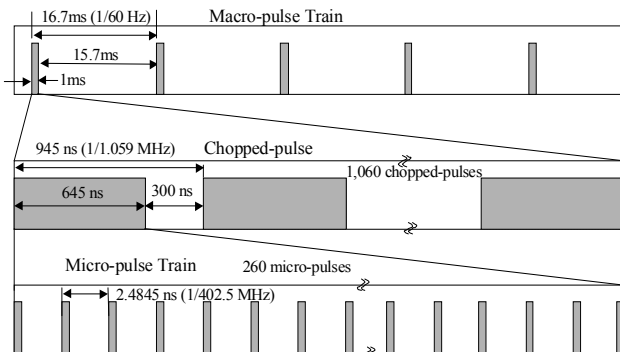


Figure 1. Time structure of the SNS beam-pulses.

\*Work supported by the Office of Energy Research, Basic Energy Science of the US Department of Energy.

The chopping system must meet several requirements: 1) the cleanliness of the beam gap must be 1 in  $10^4$  to minimize activation or damage of the ring extraction elements, 2) beam loss along the linac, including the chopper transients, must not exceed 1 W/m, and 3) the beam power dissipation on the MEBT chopper target must not exceed 400 W. Here, we look into the efficacy of the chopper-system in meeting these criteria using four different timing scenarios for the two choppers.

## 2 LEBT CHOPPER

### 2.1 Structure

The LEBT chopper is the final LEBT electrode divided into 4 sections as shown at left in Fig. 2. This segmented electrode is just upstream of the grounded entrance aperture of the RFQ at far right.

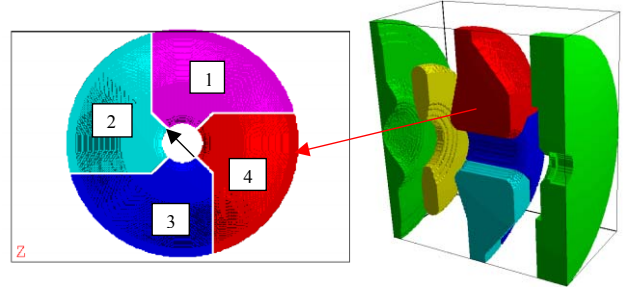


Figure 2. LEBT chopper configuration.

Collectively, the four chopper electrodes operate at -40 kV to focus the beam into the RFQ. By superimposing  $\pm 2$  kV on opposing segment pairs we can arrange to deflect the beam toward  $45^\circ$ ,  $135^\circ$ ,  $225^\circ$ , or  $315^\circ$ . During a 300-ns chopping gap, the electrodes maintain a constant orientation. Chopped beam from successive gaps will be sequentially deflected into the 1<sup>st</sup>, 2<sup>nd</sup>, 3<sup>rd</sup> and 4<sup>th</sup> quadrants. For a voltage rise and fall time of 25 ns, up to 20 micropulses in each gap may experience only partial deflection. Operating in the chopping mode breaks axial symmetry the of LEBT fields. For our beam simulation studies, we transport the beam through the 3-D fields of the LEBT.

### 2.2 Simulation

We start with an initial particle distribution derived from x and y beam emittance measurements made at slightly different longitudinal locations. We transform to the midpoint between the measurements without space charge and construct a numerical particle distribution.

This particle distribution continues backward through the LEBT to a reference point well before the deflection electrodes. This transport uses axially symmetric fields

corresponding to the chopper fields turned off. The computer code PARMELA, used for all the LEBT simulations, verifies that forward and backward beam transport with 3-D space charge is completely reversible. We begin with the particle distribution at the reference point for all of our LEBT chopper simulations.

With the chopper off, the beam arrives “matched” at the RFQ entrance. When the LEBT chopper is on, the beam enters the RFQ off-axis and off-angle depending upon the relative polarity and voltage of the chopper segments. This non-axial beam represents a serious mismatch to the RFQ resulting in significant emittance growth at its exit.

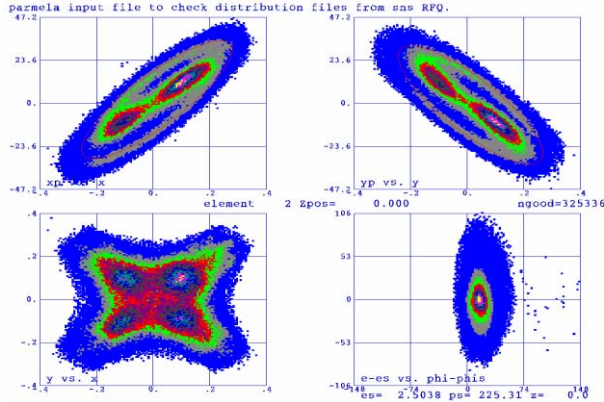


Figure 3. Superimposed phase-space distributions at the RFQ-exit for 4 partially LEBT-chopped beams.

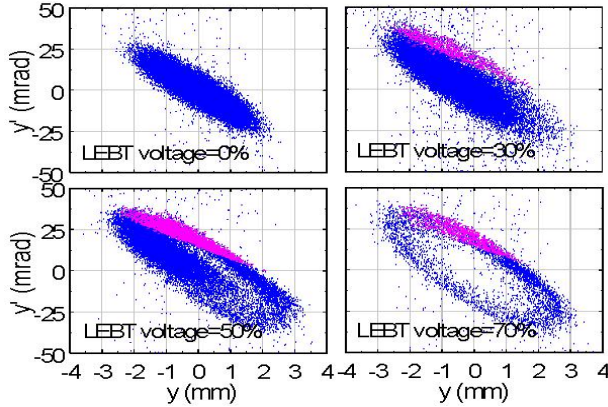


Figure 4. Phase space ( $y$ - $y'$ ) projections at the RFQ exit for different LEBT voltages.

Figure 3 shows the effective phase-space distribution of the beam at the RFQ exit for the LEBT chopper at  $\pm 1$  kV, or 50% of its maximum voltage. This figure is the superposition of four partially chopped beams, each one deflected by the LEBT chopper into a different quadrant. Because the measured beam, and consequently the initial particle distribution, is not symmetric, we find that the transmission and relative emittance growth is correlated with the direction of chop. This composite picture is representative of the beam that must be transmitted through the MEBT during the LEBT chopper voltage transients.

To simplify the study, we chose to follow only beams that have been deflected into the first quadrant by the

LEBT chopper as representative of all four cases. Figure 4 shows the evolution of the  $y$ - $y'$  phase space of this beam at the RFQ exit during the LEBT voltage ramp at 0%, 30%, 50% and 70% of maximum deflection into the first quadrant. Blue dots represent particles that have survived the RFQ. During the ramp, we see about ten-fold increase in emittance and the  $y$ - $y'$  projection transforms to a hollow ellipse.

Red dots in Fig. 4 represent the  $y$ - $y'$  coordinates of particles at the RFQ output that survived the MEBT chopper at its full voltage and appear at the entrance to the DTL. These particles represent potential contamination of the edges of the chopper gap. Because of their large effective emittance, they would likely be lost in the linac.

### 3 MEBT CHOPPER

#### 3.1 Structure

The MEBT chopper is a traveling-wave structure with a novel plate structure [3]. The deflection plates, each 35-cm long, are separated by 1.8 cm. A maximum of  $\pm 2.4$  kV applied to the plates deflects the beam upward. The rise and fall time is  $\sim 10$  ns. A quadrupole triplet magnifies the displacement and directs the beam onto the chopper target. The target is designed to handle an instantaneous power density of  $200 \text{ kW/cm}^2$  and an average power of  $400 \text{ W}$  [4]. This study addresses only the expected average power, but not the expected power density.

#### 3.2 Simulation

To tune the MEBT, we set the transport element parameters to the matched beam condition and adjust the vertical position of the chopper target to intercept just 1% of the unchopped beam (39 W average). Beam is then transported through the LEBT and its chopper using the PARMELA code, through the RFQ using the TOUTATIS code and through the MEBT and its chopper to the DTL entrance using the PARMILA code. Each stage of the calculation includes 3-D space-charge effects.

### 4 CHOPPING OPTIONS

We consider four different chopper-timing sequences illustrated in Figure 5. The left-hand column shows the relative timing and the voltage ramps of the two choppers, the LEBT chopper in red and the faster MEBT chopper in blue. The middle column shows the corresponding current in individual micropulses at the entrance to the DTL, assuming a linear relationship between voltage and beam current chopped. The right-hand column shows the current intercepted on the MEBT-chopper target during the turn-on transient.

Table 1 summarizes the relative virtues of the four options. In option 1, the MEBT chopper turns on first to minimize stray beam entering the linac. However, this scenario results in the maximum power dissipation on the chopper target. In option 2, the LEBT chopper turns on first so that no beam ever gets deflected onto the MEBT target. This option results in no power deposited in the

chopper target but maximizes the amount of beam lost in the linac. In option 3, the voltage ramps start together while in option 4, ramps end at the same time. To test the linear model we simulated the beam dynamics performance for option 1 using  $10^6$  macroparticles transported from the LEBT to the DTL.

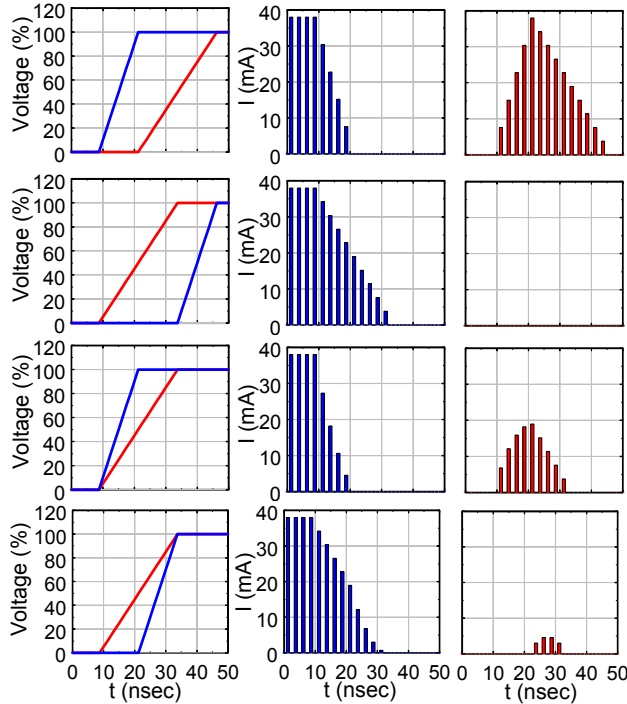


Figure 5. Chopper timing options showing LEBT and MEBT voltage ramps, micropulse current in the falling edge of the chopper gap and micropulse current on the chopper target.

Table 1. Linear model predictions and simulation.

chopper timing option	average linac current during transient ( $\mu\text{A}$ )	average MEBT target power dissipation (W)
1	24	226
2	54	0
3	19	87
4	49	12
simulation	16	208

Figure 6 shows the y-y' emittance at the DTL entrance for four voltages of MEBT acting alone. The asymmetry of the unchopped beam reflects the missing 1% removed by the chopper target. During the MEBT transient, the beam entering the linac nominally remains within the phase space defined by the matched beam. However, even at full chopper voltage  $\sim 16 \mu\text{A}$  (peak) enters the linac, which fails to meet the gap-current goal.

Turning on the faster MEBT chopper first, maximizes the gap length and minimizes the potential for losing partially chopped bunches in the linac. Turning on the LEBT chopper first decreases the beam current entering the MEBT, but it spoils the emittance (see Fig. 4) allowing more beam past the MEBT target. The left plot in Fig. 7 is a log-scale histogram showing current entering the DTL for simulation of option 1. The right plot shows

the number of particles striking the MEBT target. The DTL input beam increases briefly during the LEBT voltage transient. With both choppers at full voltage, only  $\sim 31 \text{ nA}$  peak current (12 of  $10^6$ ) enters the DTL, easily meeting the gap cleanliness requirement. The average power dissipation in the MEBT target of 208 W (in addition to 39 W intercepted all the time) meets the target power design limitation.

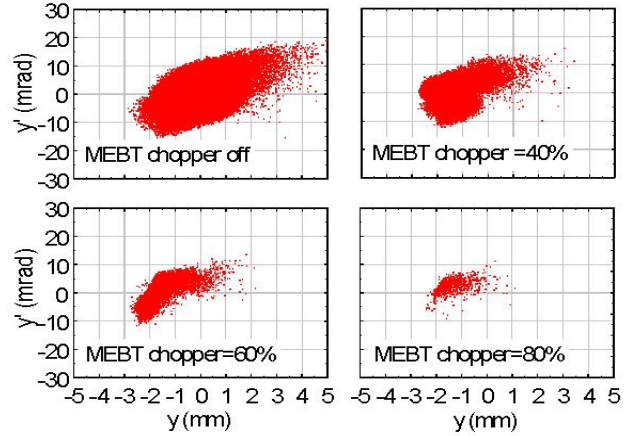


Figure 6. Particle coordinates (y-y') at the DTL input for various MEBT chopper voltage when acting alone.

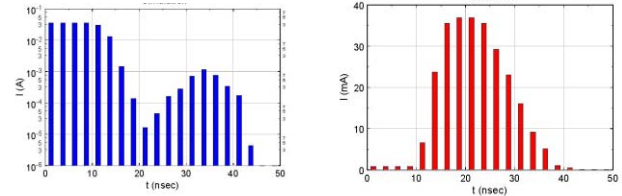


Figure 7. Simulated beam current vs. time for option 1 at the DTL input (left) and the chopper target (right).

## 5 CONCLUSION

Of the four options studied using a linear model, option 3 is most attractive because it minimizes the potential beam loss in the linac while easily meeting the chopper-target power limitations. While only option 1 was confirmed by beam-simulation, we expect similar results for option 3. Partially chopped beam lost at or near the DTL entrance corresponds to less than 0.1 W, meeting the beam-loss limit of 1 W/m.

## 6 REFERENCES

- [1] J. Staples et al., "The SNS Front-end Accelerator Systems," Proceedings of the XIX International Linac Conference, 1998, Chicago, IL, USA.
- [2] J. Stovall, J. H. Billen, S. Nath, H. Takeda, L. M. Young, D. Jeon, R. Shafer, and K. Crandall, "Expected Beam Performance of the SNS Linac," Proceedings of the 2001 Particle Accelerator Conference, p 446, June 18-22, 2001, Chicago, IL, USA.
- [3] S. S. Kurennoy et al., "Progress with SNS fast beam chopper," p 1435, *ibid*.

- [4] D. Oshatz et al., "Mechanical design of the SNS  
MEBT," p 1574, ibid.